SPACECRAFT ANOMALY ANALYSIS AND PREDICTION SYSTEM – SAAPS

P. Wintoft[1)], H. Lundstedt[1)], L. Eliasson[2)], L. Kalla[2)], and A. Hilgers[3)]
1) Swedish Institute of Space Physics – Lund Division
2) Swedish Institute of Space Physics – Kiruna Division
3) ESA, ESTEC, Noordwijk

14 April 2001

Abstract

A spacecraft anomaly analysis and prediction system (SAAPS) is under development. The three main modules of SAAPS are: 1) a database of space environment data and spacecraft anomalies, 2) tools to analyze the space environment at times of anomalies, 3) models to predict the environment and anomalies. The database will contain solar wind data, magnetospheric particle flux data, and geomagnetic indices. The database is updated in real time. The analysis module consists of different statistical and neural network tools that should help to identify the cause of anomalies. The prediction module contains statistical and neural network models to predict various space environment parameters and spacecraft anomalies. As the database is updated in real time this also enables forecasting. In this work we describe the various parts of SAAPS.

1 Introduction

This paper describes the ongoing development of a Spacecraft Anomaly Analysis and Prediction System, hereafter called SAAPS. SAAPS is part of the ESA funded project *Development of AI methods in spacecraft anomaly predictions* (ESTEC contract 11974/96/NL/JG(SC)). The project is a continuation of the ESA *Study of plasma and energetic electron environment and effects* [8]. As the title indicates, we aim at developing a computer system that enables users to analyse the space weather at times of anomalies, and to predict anomalies.

Many years of experience exist on how spacecraft are affected by the space environment. These findings have been included in the design of spacecraft to reduce the risks of anomalies related to surface charging [10] and internal charging [9]. However, the properties of the plasma and radiation that surrounds the spacecraft vary dramatically both over space and in time. Thus, it is difficult to completely remove anomalies related to the space weather [18].

On most spacecraft anomalies occur regularly. Their impacts are often not dramatic, but they still have to be dealt with, and may also include intervention from on-board systems or ground control. However, there are also severe events such as the failures of the momentum wheel control systems on ANIK E1 and E2 in 1994 [1, 2] and the loss of solar power on E1 in 1996 [3].

There are several related projects that study the space weather and its effects on spacecraft. The Space Environment Information System (SPENVIS) [6, 13] contains an impressive number of models, and not only for spacecraft charging purposes. The intended users of SPENVIS are spacecraft engineers, scientists, and educators and students. A specific model to study internal charging is DICTAT [12]. DICTAT is also one of the models included in SPENVIS.

In the rest of the paper we will describe SAAPS and its subsystems and also discuss the results of the analysis and prediction of a few selected anomaly sets.

2 SAAPS

One difficulty in analysing or predicting space weather related effects is the collection of necessary data. Many data sources exist with their specific formats. The data can be publicly available over the Internet or distributed on CD-ROMs. Even doing a simple summary plot of a few selected parameters can be quite time consuming. One of the goals with SAAPS is to set up a database that contain most of the available data that can be used for analysing and predicting spacecraft anomalies, especially those related to charging events. Having this database, the data is then directly available to the models. Below we describe the SAAPS database and give examples of possible analysis and prediction tools, and how SAAPS is implemented.

2.1 Database

The database consists of space environment data and spacecraft anomaly data. The space environment data are made up of solar wind plasma data, geostationary electron and proton flux data, and geomagnetic indices.

The data is retrieved from the database by specifying a parameter, e.g. ACE B_z, and the time period. This will result in what we define as a Time Series Object (TSO). The TSO contain the meta data, e.g. field names and units, together with the data. All the models and tools then operates on the TSOs.

The current status of the space environment data in the database is summarized below. Several items are updated in real time that enables nowcasting and forecasting.

Solar data

From the GOES-8 and -10 satellites the X-ray observations are included. The data has a time resolution of 5 minutes and the SAAPS database is updated every 10 minutes. The X-ray flux data are measured in two wavelength bands: 0.05-0.4 nm and 0.1-0.8 nm.

Solar wind data

Both the ACE and OMNI solar wind data are included. The ACE data consist of particle density, velocity, and the three magnetic field components. The data has a time resolution of 1 minute and are downloaded in real time every 10 minutes. The data extends from March 2000 up to present. The OMNI data extends over the period January 1982 to December 1999 and consist of one hour resolution solar wind density, velocity, magnetic fields, and proton fluxes from $>$ 1 MeV to $>$ 60 MeV.

Magnetospheric particle data

GOES-8, -10, and LANL 1990-095 particle data are included. The GOES electron flux cover three energy levels: $>$ 0.6 MeV, $>$ 2 MeV, and $>$ 4 MeV. The $>$ 4 MeV range is mostly empty. The proton flux cover 6 energy levels: $>$ 1 MeV, $>$ 5 MeV, $>$ 10 MeV, $>$ 30 MeV, $>$ 50 MeV, and $>$ 100 MeV. The GOES data has a time resolution of 5 minutes and are updated every 10 minutes. Only the electron flux data for a few selected energy levels from the LANL satellite has been included in the SAAPS database. The data has also been averaged to 1 hour resolution. The selected energy levels are about: 20 eV, 100 eV, 1 keV, 10 keV, 100 keV, 1 MeV, and 10 MeV. The data extends over the period January 1996 to December 1998.

Magnetospheric indices

The Kp, Dst, and AE indices are included. The Kp index is updated in real time with both the estimated Kp from SEC, and the nowcasted and forecasted Kp from Lund Space Weather Center. The Kp index extends back to 1970. The Dst index extends over the period 1957 to December 2000. Currently it is not updated in real time. The AE index extends over the period 1957 to 1988.

Anomaly data

The spacecraft anomaly data comes from several different spacecraft that are mainly in geostationary orbits. Due to confidentially issues only very limited information about the anomaly data set will be given here.

There is a total of about 10 000 anomalies in the data set. The data comes from several different satellites. The set extends from around 1970 up to present. There is usually a short description for each reported anomaly, describing either on what part of the satellite the anomaly took place or the probable physical cause of the anomaly. The physical causes can be single event upset (SEU) or electrostatic discharge (ESD), were ESD can be either due to surface charging or internal charging.

2.2 Analysis system

The analysis system shall provide the user to do on-the-fly analysis of space weather data that are related to spacecraft anomalies. The interface is a web browser that supports Java Applets. In the following we will present some of the tools in the analysis system.

Plotting tool

The plotting tool can be used to plot any space weather data that exist in the SAAPS database or from user submitted data. From the plot interface (Figure 1) the user can inspect the space weather data in the database, upload data for a specified time period, and to create a plot. When the *Plot* button is pushed the plot appears in a separate window (Figure 2). The plot can be further manipulated by changing the plot style, changing the axis scaling and limits. It is also possible to zoom into the plot so that details can be studied.

Superposed epoch analysis

In the above case the user explicitly specified a start and end data over which data should be plotted. Another approach for multiple event studies is to use superposed epoch analysis. The user now submits a list

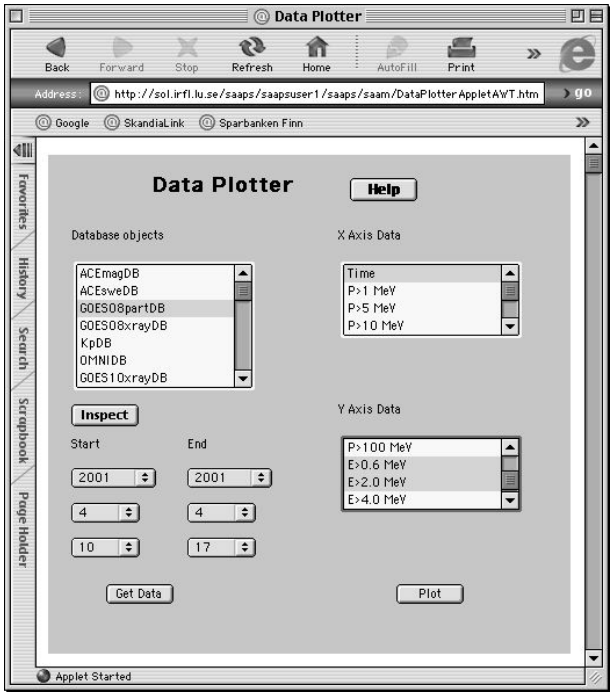

Figure 1: The interface to the plot tool. Here it is shown how the user has selected GOES-8 particle data for a period in April 2001 to create a plot with time on the x axis, and the > 0.6 and > 2 MeV electron flux on the y axis. Pushing the *Get Data* button uploads the data for the selected time period from the SAAPS server. The *Plot* button creates the plot in a separate window.

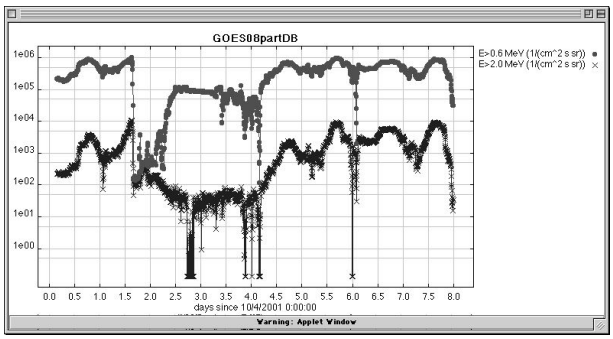

Figure 2: The resulting plot window from the selection shown in Figure 1. The labels to the right are created from the meta data in the time series object. Attached to the window (not shown here) are pull-down menus that can be used to select plot style, axes scaling, etc.

of events. For each event data is uploaded for a time period around the event and all the time segments of data are averaged. Figure 3 shows the interface to the superposed epoch analysis tool. The user enters a list of anomaly events, in this case four events in the beginning of 1996. The parameter to be studied is then selected, and in this example the GOES-8 > 2 MeV electron flux data has been selected. The event window then defines how far back and forward in time, centred on each event, data shall be uploaded (here, -3 days to 2 days). The superposed events can then be plotted as shown in Figure 4. The figure clearly shows the typical rise in energetic electron flux prior to anomalies related to internal charging. The $\pm$ one standard deviation are also plotted. The result can also be compared to that obtained from a list of random events. In Figure 3 five random events have been selected automatically from the total time span of the four anomaly events. The resulting plot is shown in Figure 5. As espected, the figure shows the typical diurnal variation with no trends based on the random events. This also indicates that the increase in the electron flux in Figure 4 is significant.

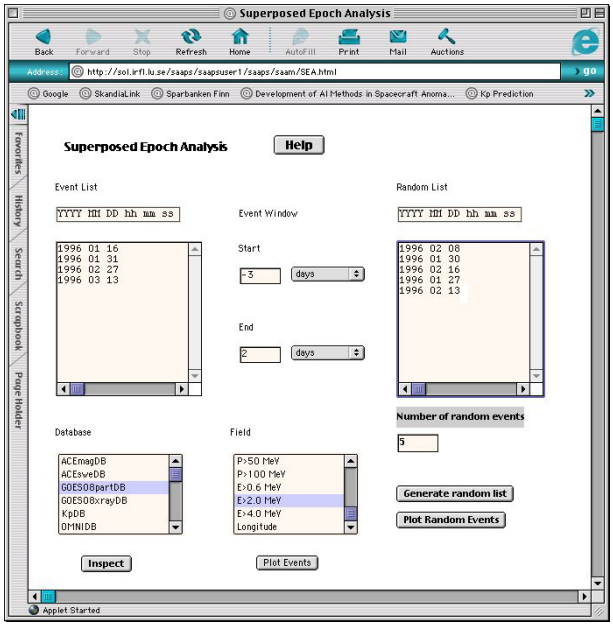

Figure 3: The superposed epoch analysis interface. Description is given in the text.

Linear correlation and mutual information

Linear correlation and mutual information can also be calculated from the anomaly list and the SAAPS data. The linear correlation on a data set is a number between -1 and +1, where -1 means perfectly anticorrelated, +1 perfectly correlated, and 0 uncorrelated. However, linear correlation assumes a linear model. Mutual information is a number between 0 and 1,

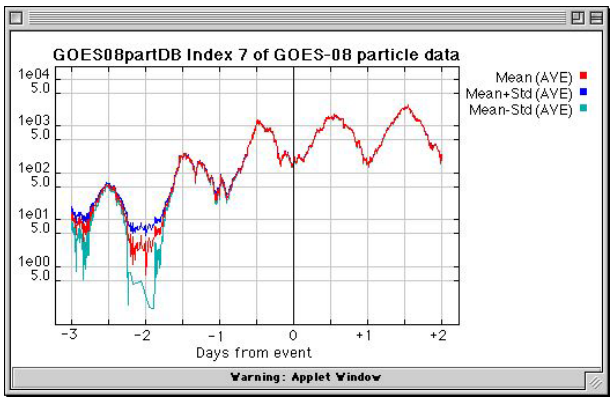

Figure 4: The average and the ± one standard deviation of the GOES-8 > 2 MeV electron flux for the four anomaly events.

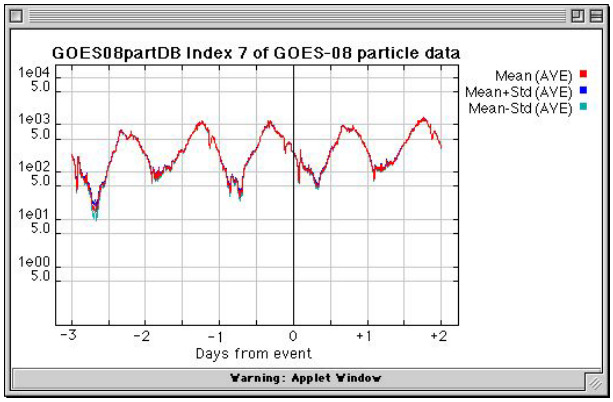

Figure 5: The average and the ± one standard deviation of the GOES-8 > 2 MeV electron flux for the five random events.

where 0 means no correlation and 1 perfect correlation. The mutual information measure assumes nothing about the model, thus whether it is linear or non-linear. Thus, although two parameters can be weakly linearly correlated they might be strongly non-linearly correlated. Here we will use the mutual information to study the relationship between a daily geomagnetic storm index and daily anomaly data.

We use $\sum$Kp as it is available in real time, it covers many years, and there are no data gaps. It can be used to study ESDs related to internal charging due to its correlation with the energetic electron flux at geosynchronous orbit [7, 14, 18].

From the SAAPS anomaly database we select five sets, named S1 through S5. Each set contain both SEUs and ESDs, except set S5 that contain only SEUs. We define a "no anomaly" event as an event for which no anomalies occur during a UT day. A "anomaly" event is defined as an event for which one or more anomalies occur during a UT day.

The mutual information between the two random variables X and Y is defined as [15]

$$I(X;Y) = \sum_{i=1}^{m}\sum_{j=1}^{n} p(x_i, y_j) \ln \frac{p(x_i, y_j)}{p(x_i)p(y_j)}. \quad (1)$$

Here $p(x_i)$ is the probability that X has the value x_i, and $p(y_j)$ is the probability that Y has the value y_j. $p(x_i, y_j)$ is the joint probability. The use of ";" in Equation 1 means that X and Y are interchangeable, i.e. $I(X;Y) \equiv I(Y;X)$. The mutual information $I(X;Y)$ is then normalized with the entropy of Y to get the relative mutual information

$$I_r(X,Y) = \frac{I(X;Y)}{H(Y)}, \quad (2)$$

where the entropy $H(Y)$ is defined as

$$H(Y) = -\sum_i p(x_i) \ln p(x_i). \quad (3)$$

The relative mutual information $I_r(X,Y)$ has a value of between 0 and 1, where 0 means that the two variables are uncorrelated and 1 means that they are perfectly correlated. Using mutual information instead of linear correlation has the advantage that there is no assumption about a linear model.

We set X to the average of $\sum$Kp over d days $\langle \sum \mathrm{Kp} \rangle_d$. Y is set to 0 if there are no anomalies during a day, and 1 if there are at least one anomaly during the day. We bin the $X = \langle \sum \mathrm{Kp} \rangle_d$ values into 8 bins and the Y values fall naturally into two bins. By letting d vary from one day to ten days we calculate I. The result is shown in Figure 6. We see that the different anomaly sets show different behaviour on $\langle \sum \mathrm{Kp} \rangle_d$. The S5 anomaly set shows no (linear or non-linear) correlation to $\langle \sum \mathrm{Kp} \rangle_d$. The

other anomaly sets show some relation to $\langle \sum \mathrm{Kp} \rangle_d$ but with the strongest correlation for different time lag d.

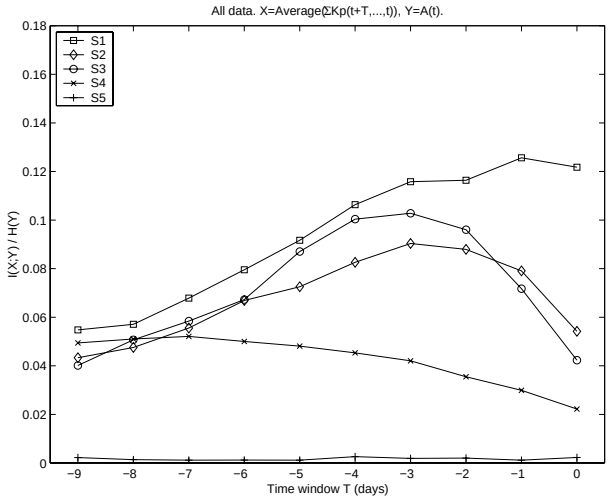

Figure 6: The relative mutual information $I(X;Y)/H(Y)$ for the five different anomaly sets as a function of d. The anomaly sets contain all the anomaly data.

Next we remove all data that are not classified as electrostatic discharges (ESD) and calculate the mutual information again. The S5 anomaly data are completely removed as it consist only of single event upsets (SEU). This is the reason why the mutual information in Figure 6 was close to zero. The calculations for the ESD data are shown in Figure 7. The correlations are generally stronger, but there is still a large discrepancy on the variation on d, that will be addressed in the Discussion section.

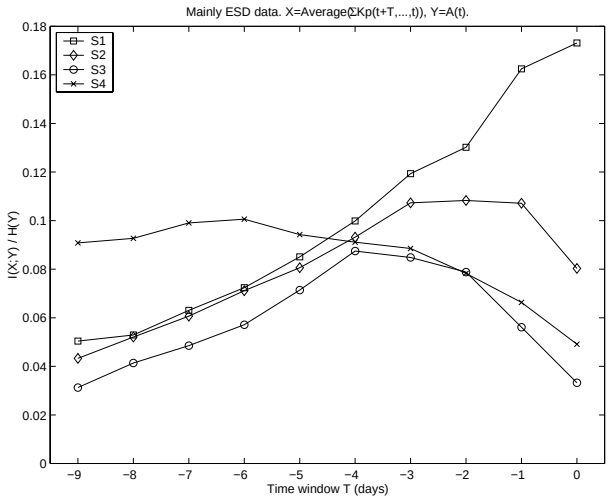

Figure 7: The relative mutual information $I(X;Y)/H(Y)$ for the five different anomaly sets as a function of d. The anomaly sets contain only ESD data.

Other tools

If local time information is available in the anomaly data (geostationary satellites) then a histogram tool can be used to analyse the local time distribution of the events.

The prediction system, that will be described in the next section, can be accessed by the analysis system. This enables the user to submit a list of events that then can be matched against several different prediction models. Each model has the capability of predicting a certain type of anomaly. The tool suggests the model that best matches the anomaly data. Two things can come out from this analysis. Firstly, the user submitted anomalies can be compared to known anomalies described by the models. Secondly, the user will have access to a forecasting model that predicts anomalies that are similar to the submitted anomalies.

2.3 Prediction system

Based on the space environment data several different models are developed to predict the anomaly data. Both statistical methods and neural network algorithms are used.

Spacecraft operators generally avoid sending commands during times of high anomaly rates [3]. Having a model that can forecast or nowcast times of increased risk of anomalies enables the operators to act at an earlier stage.

Threshold model

It has been shown that the daily, or two day, fluence of energetic electrons are related to internal charging anomalies [18]. By taking the daily GOES-8 > 2 MeV electron fluence threshold levels can be assigned that indicates increased risk of internal charging. Figure 8 shows this model implemented in SAAPS. The levels defined [*Wrenn, Private comm.*] indicates low risk (green), medium risk (yellow), or high risk (red). The figure shows the situation over eight days in April 2001.

Anomaly prediction model based on $\sum$Kp

Based on the results from the previous section we develop a model for the prediction of S1 anomalies using $\sum$Kp as input. As the S1 anomalies are strongest related to the current $\sum$Kp the best result will be achieved for a nowcasting model. It is also probable that the anomaly not only depends on the current $\sum$Kp but also on the history of $\sum$Kp. However, we do not know how far back in time we need to go. We

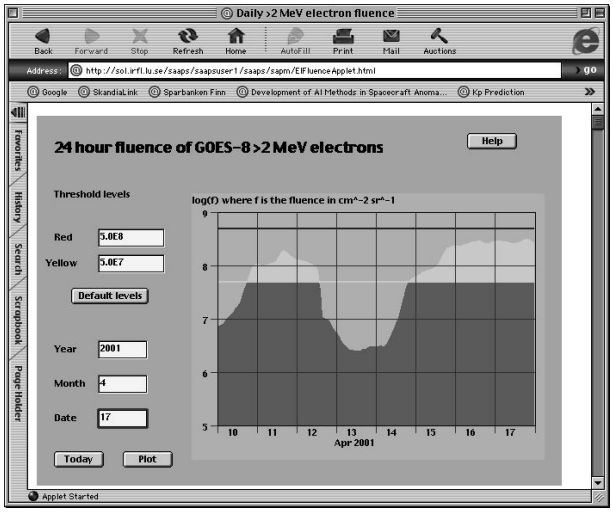

Figure 8: The plot shows the daily fluence levels of the GOES-8 > 2 MeV electrons for April 10–17, 2001. The threshold levels are set at 510^7 and 510^8 cm^{-2} sr^{-1} for the yellow and red levels, respectively. In this figure green is represented with dark grey, yellow with light grey, and red with black. The fluence is at "yellow" levels around 11 April and from the evening of 14 April and onwards.

let the input to the model be the vector

$$\mathbf{x} = \begin{bmatrix} x_1 \\ \vdots \\ x_{m-1} \\ x_m \end{bmatrix} = \begin{bmatrix} \sum Kp(d-D) \\ \vdots \\ \sum Kp(d-1) \\ \sum Kp(d) \end{bmatrix}, \quad (4)$$

where D is varied from 0 to 9 days. The inputs are normalized so that they fall in the range [-0.8,+0.8]. The output is whether there is an anomaly or not during the day

$$y(d) = \begin{cases} -0.8 & 0 \text{ anomalies during day } d \\ +0.8 & > 1 \text{ anomalies during day } d \end{cases}. \quad (5)$$

The model is a feed-forward neural network with one hidden layer [15]. The equation for the model is

$$z = \tanh\left(\sum_{j=1}^{n} w_j \tanh\left(\sum_{i=1}^{m} v_{ji}x_i + a_j\right) + b\right), \quad (6)$$

where v_{ji}, a_j, w_j, and b are the weights (free parameters) of the neural network. The weights are found using a training algorithm in which an input $\mathbf{x}$ is presented and the output z is calculated. The difference between the calculated output and the observed output y is used to update the weights so that the difference becomes smaller. This is repeated a large number of times for all the data in the training set. The training is stopped when a minimum in the RMS error is reached calculated on an independent data set called the validation set. The procedure is repeated by varying the number of hidden neurons (n) and the number of inputs ($m = D+1$). The network with the lowest validation error have $D = 7$ days (eight inputs) and $n = 3$ hidden neurons. However, the performance of the model is not very sensitive on the time delay D, the variation in RMS errors are larger for different initial weights. But we still choose the optimal network to be the network that has the minimum validation RMS error.

We may now compute the overall probabilities that the model make correct predictions based on the training, validation, and test sets. It turns out that the performance of the model is quite similar for the three sets, and we can therefore compute the probabilities for the set containing all three sets. The result is summarized in Table 1. From the table, we see that both the probability that a predicted event is actually observed ($P(t|y)$), and that an observed event is correctly predicted($P(y|t)$) , are slightly higher than 70% .

Table 1: The conditional probabilities $P(t|y)$ for the nowcast network computed on the data set containing the training set, validation set, and test set. The observed output is t and the predicted output is y. The anomalies are class A and the no anomalies class B.

$P(t = B\|y = B)$	0.728
$P(t = A\|y = A)$	0.714
$P(y = B\|t = B)$	0.706
$P(y = A\|t = A)$	0.736

One might expect that the overall probability of 70% contain events that have no clear relation to $\sum$Kp and events that are well correlated to $\sum$Kp. We can then ask the question: Is there a way of estimating the correctness of a prediction from the model? To investigate this we see that the model output from Equation 6 is a number between -1 to +1, as the tanh function limits the output. In the ideal case the model will produce -0.8 for a "no anomaly" event and +0.8 for an "anomaly" event. But in practice the output will thus take on any value between -1 and +1, and when the output is close to 0 it is probable that the prediction is poor. We can examine if this is really the case by calculating the probabilities as a function of model output. The result is shown in Figure 9. The absolute value of the predicted output have been binned into the five bins with limits $0, 0.125, 0.25, 0.375, 0.5, \infty$ and the probabilities have been calculated in each bin. It is clear from the figure that model outputs with values close to 0 give predictions with probabilities around 50% , i.e. close to guessing. The probabilities then increases monoton-

ically for model outputs of increasing absolute values. When the output is below -0.5 or above +0.5 the probability that the prediction is correct is 85% or higher.

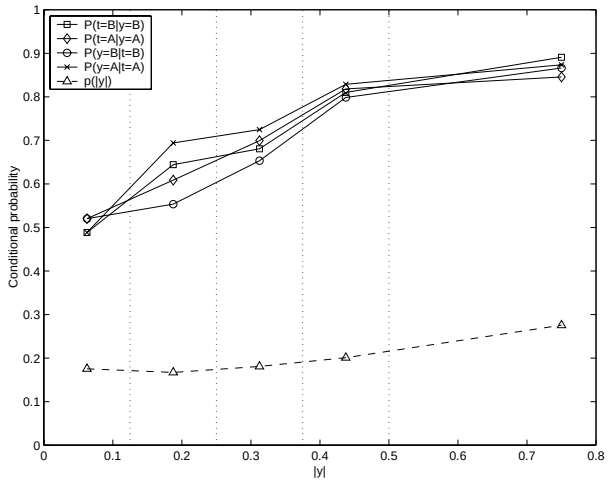

Figure 9: The conditional probabilities calculated in five bins. Each bin contain data with model absolute output values ($|y|$) in the range indicated by the vertical dotted lines. The dashed curve shows the fraction of examples in each bin ($p(|y|)$).

2.4 Implementation

At the start of the project it was decided that the tools should be available over the Internet using a web browser. There are many ways to achieve this but we decided to use Java [5] as it means that we only need to use one programming language. However, there are several other advantages of using Java as it is a modern object oriented language. Java is made up of several different packages. One package contain Applets. An Applet is a program that can be executed from within a web browser such as Netscape or Microsoft Internet Explorer. Another package contain Remote Method Invocation (RMI) that enables the Applet in the web browser to start programs on the web server from which the Applet was loaded. A typical tool in SAAPS contain a user interface from which models, data, time intervals, etc., can be selected. The user interface is an Applet. When the user pushes a button that e.g. will fetch data from the SAAPS server this is accomplished with RMI.

Java is platform independent. This means that when the program is compiled it can run on any machine without recompiling the code. However, to run any Java programs a Java Virtual Machine (JVM) must be installed. The JVM acts as a translating layer between the compiled Java code and the computers operating system.

3 Discussion and conclusions

It was seen from Figure 7 that the time dependency on $\sum$Kp for the four anomaly sets were different. All the anomalies were classed as ESDs. However, from other studies it has been shown that the S1 set are ESDs due to surface charging, and the sets S2 and S3 are internal charging. The S4 set contain a mixture of ESD anomalies. The time dependency on $\sum$Kp can thus be used for an analysis tool to suggest whether the likely causes for a new anomaly set are surface charging or internal charging. Note also that the time resolution of the anomalies are one day, thus no positional information is needed for the satellite as long as it is geostationary.

The prediction model for the S1 set is thus a model for surface charging anomalies. Other models will be developed for the prediction of other anomaly sets, and thus for both surface and internal charging anomalies. The prediction models can be combined with analysis tools to find the probable cause of a user provided anomaly or set of anomalies.

The prediction models for spacecraft anomalies will in the future be further developed to include other spacecraft anomaly lists. It will also be studied whether models can be developed to predict the anomalies with a better time resolution than one day. E.g., anomalies related to internal charging on geosynchronous satellites are caused by MeV electrons [19], and the MeV electron flux could be used as input to a model. To push the prediction horizon further solar wind data monitored at L1 can also be used as input. It has already been demonstrated that the geosynchronous MeV electron flux can be predicted from solar wind data [17].

The approach of SAAPS to try to collect data into one database is somewhat old fashioned. If instead all the different institutes and organizations defined a common interface over which the data could be accessed much more time could be spent on using and analysing the data. Scientists could then develop tools that collects data from many different places around the world without having to go through the process of translating between different formats. Different techniques exist that can solve this, and where Java is very well suited. The DataGrid project [4] is an EU funded initiative to develop the technology for distributed databases and programming. It will be very interesting to see if that project can be used for the space weather applications.

Acknowledgements

The following organizations and individuals are highly acknowledged for providing data: SEC, NOAA, ESTEC, Terry Onsager (SEC), and Geoff

Reeves (LANL). Gordon Wrenn is acknowledged for discussion on the threshold levels for the daily electron fluence.

References

[1] *Aviation Week & Space Technology*, p. 28: ANIK E2 Disabled, Jan. 31, 1994a.

[2] *Aviation Week & Space Technology*, p. 58: Telesat Starts ANIK E2 Rescue Effort, Feb. 7, 1994b.

[3] Baker, D.N., J.H Allen, R.D. Belian, J.B. Blake, S.G. Kanekal, B. Klecker, R.P. Lepping, X. Li, R.A. Mewaldt, K. Ogilvie, T. Onsager, G.D. Reeves, G. Rostoker, R.B. Sheldon, H.J. Singer, H.E. Spence, and N. Turner, An Assessment of Space Environmental Conditions During the Recent Anik E1 Spacecraft Operational Failure, *ISTP Newsletter, 6*, No. 2, June, 1996.

[4] *The DataGrid Project*, http://www.eu-datagrid.org/ .

[5] Gosling, J., *The Java Language Specification*, Addison Wesley Publ. Comp., 2000.

[6] Heynderickx, D., B. Quaghebeur, E. Speelman, E.J. Daly, ESAs SPace ENVironment Information System (SPENVIS): A WWW Interface to Models of the Space Environment and its Effects, *38th Aerospace Sciences Meeting & Exhibit, 10-13 January 2000, Reno, NV* , AIAA 2000-0371, 2000.

[7] Koons, H.C., and D.J. Gorney, Relationship between electrostatic discharges on spacecraft P78-2 and the electron environment, *J. Spacecraft and Rockets, 28*, 683–688, 1991.

[8] Koskinen, H., L. Eliasson, B. Holback, L. Andersson, A. Eriksson, A. Mlkki, O. Norberg, T. Pulkkinen, A. Viljanen, J.-E. Wahlund, and J.-G. Wu, *Space Weather and its Interactions with Spacecraft*, Summary report of *Study of plasma and energetic electron environment and effects*, ESTEC/Contract No. 11974/96/NL/JG(SC), 1998.

[9] Mulville, D.R., *Avoiding problems caused by spacecraft on-orbit internal charging effects, NASA Technical Handbook*, NASA-HDBK-4002, Feb. 17, 1999.

[10] Purvis, C.K, H.B. Garret, A.C. Whittlesey, N.J. Stevens, *Design Guidelines for Assessing and Controlling Spacecraft Charging Effects*, NASA Technical Paper 2361, 1984.

[11] Rodgers, D.J., Correlation of Meteosat-3 anomalies with data from the spacecraft environment monitor, *Internal ESTEC Working Paper No. 1620*, E.W.P. 1620, Noordwijk, 1991.

[12] Rodgers, D.J., *Engineering Tools for Internal Charging, Final Report*, DERA/CIS/CIS2/CR990401, 1999.

[13] *SPace ENVIronment Information System – SPENVIS*, http://www.spenvis.oma.be/spenvis/ .

[14] Stringer, G.A., I. Heuten, C. Salazar, and B. Stokes, Artificial neural network (ANN) forecasting of energetic electrons at geosynchronous orbit, *Radiation Belts: Models and Standards, Geophys. Monograph 97*, AGU, 291–295, 1996.

[15] Swingler, K., *Applying Neural Networks, A Practical Guide*, Academic Press Limited, London, 1996.

[16] Wilkinson, D.C., *Spacecraft Anomaly Manager*, NOAA, NGDC, Solar-Terrestrial Physics Division, Boulder, 1994.

[17] Wintoft, P., and H. Lundstedt, Neural network prediction of geosynchronous relativistic electron flux from solar wind data, *The First S-RAMP Conference, Sapporo, Japan, Oct. 2-6, 2000*, S1-P11, p. 22, 2000.

[18] Wrenn, G.L., Conclusive evidence for internal dielectric charging anomalies on geosynchronous communications spacecraft, *J. Spacecraft and Rockets, 32*, 514–520, 1995.

[19] Wrenn, G.L., and A.J. Sims, Internal charging in the outer zone and operational anomalies, *Radiation Belts: Models and Standards, Geophys. Monograph 97*, AGU, 275–278, 1996.